Electronic structure, elastic properties, surface energies, and work functions of NiGe and PtGe within the framework of density-functional theory for various surface terminations

Manish K. Niranjan, Leonard Kleinman, and Alexander A. Demkov*
Department of Physics, The University of Texas at Austin, Austin, Texas 78712, USA
(Received 23 October 2006; published 28 February 2007)

We present a comprehensive theoretical study of the electronic structure, elastic properties, surface energies, and work functions of NiGe and PtGe within the framework of density functional theory (DFT). Our calculated lattice constants are within 1–2% of recently reported experimental values. Calculated work functions for the (001) surfaces of NiGe and PtGe are 4.57 and 4.83 eV, respectively, suggesting that both metals and their alloys can be used as self-aligned contacts to *p*-type germanium. We identify the growth conditions necessary to stabilize this orientation. We report on an unusual surface reconstruction of the NiGe(101)–Ge-terminated surface.

DOI: 10.1103/PhysRevB.75.085326 PACS number(s): 73.61.At, 71.55.Ak, 71.20.Be, 71.20.Nr

I. INTRODUCTION

Unlike metal silicides,[1] metal germanides have not, until recently, attracted much attention, presumably due to the lack of practical applications. However, this is about to change, as scaling of traditional silicon-based technology reaches its physical limit, a germanium channel field effect transistor (FET) is generating a lot of interest.[2–6] It is worth noting that the first (bipolar) transistor of Bardeen and Brattain was made of Ge.[7] The germanium channel metal oxide semiconductor FET (MOSFET) offers high mobility of both carriers (electrons and holes), resulting in higher overdrive current, enhanced transconductance, and higher cutoff frequencies as compared with a Si transistor. Historically, the use of germanium has been limited due to the lack of a stable native oxide and processing technology. Ironically, the emerging use of alternative high-*k* dielectrics as the gate insulator in Si-based technology[8] may help finally realize the full potential of a germanium MOSFET.[5,6] Nevertheless, to fully exploit transport properties of germanium, a low-resistance contact technology will have to be developed based on metal germanides, much in the same way that self-aligned metal silicides are used in a standard complimentary metal oxide semiconductor (CMOS) process today. Thus, germanides with low *n*- and *p*-type Schottky barriers to the germanium channel (for use in NMOS and PMOS devices) need to be identified. Germanides are closely related to analogous silicides in respect to their compositions and structures. Again, with the exception of a few early papers there is no theoretical work in this area. In fact, there are not many experimental data available up to now, since in contrast to metal silicides (IrSi, PtSi, etc.) the germanides have been scarcely studied. In particular, nothing is known about the work function dependence on the crystal orientation, or the microscopic details of the Schottky barrier height (SBH) formation. Germanides have complex phase diagrams with partial solubility and a combination of multiple eutectic and peritectoid behavior, and *ab initio* calculations are extremely useful in providing fundamental understanding of the relationship between the chemical composition, bulk crystal structures, and interface structure of the alloy/semiconductor system on one hand and the SBH on the other hand. In the deep submicrometer regime (22 nm and below), NiGe, PtGe, and their alloys appear to be promising as low barrier contacts to *p*-type germanium.[9–11]

We have studied the electronic structure and calculated elastic constants of orthorhombic monogermanides NiGe and PtGe using density functional theory (DFT). We have also calculated work functions and surface energies for various surface orientations of NiGe and PtGe. Because both the local density approximation (LDA) and generalized gradient approximation (GGA) density functionals result in Ge becoming a zero gap semiconductor, if the spin orbit interaction is included, or a very narrow (~0.1 eV) direct gap semiconductor if it is not, it would require a much more esoteric[12] density functional to calculate any Ge Schottky barrier height. The rest of the paper is organized as follows. In the next section, we review bulk properties of NiGe and PtGe. In Sec. III, we report elastic constants of both the systems. In Sec. IV and V, we report and discuss the surface energies and work functions for different surface orientations.

II. CRYSTAL AND ELECTRONIC STRUCTURE OF BULK NiGe AND PtGe

All the calculations are done using density functional theory[13,14] with the projected augmented wave (PAW)[15] method as implemented in the VASP code.[16] The Perdew–Burke–Ernzerhoff (PBE)[17] form of the generalized gradient approximation for exchange and correlation is employed, along with a standard plane wave basis set with a kinetic energy cutoff of 380 eV. We use a $12\times12\times16$ Monkhorst–Pack[18] *k*-point mesh in the orthorhombic cell for the Brillouin zone integration. The calculations are converged to 10^{-6} eV/cell and the structures are relaxed until the forces are less than 0.01 eV/Å.

Both NiGe and PtGe crystallize in the primitive orthorhombic structure in a MnP-type lattice with space group *Pnma* (no. 62 in the international x-ray table)[19–22] (see Fig. 1). For NiGe, the experimental lattice constants are $a=5.84$ Å, $b=5.36$ Å, $c=3.50$ Å.[19] The PtGe experimental lattice constants are $a=6.159$ Å, $b=5.832$ Å, $c=3.754$ Å.[20] There are four symmetry equivalent Ni (Pt) and four sym-

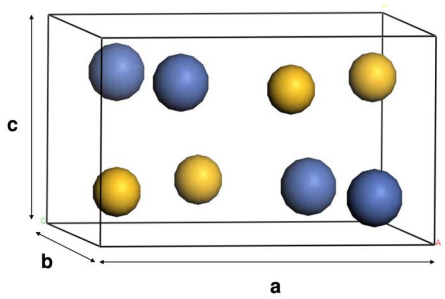

FIG. 1. (Color online) The orthorhombic unit cell of bulk NiGe and PtGe. The smaller yellow and larger blue balls are Ge and Ni atoms, respectively. Lattice constants and free internal in-plane coordinates are given in Tables I and II.

metry equivalent Ge atoms per primitive orthorhombic cell of NiGe (PtGe), respectively. There are four internal plane parameters, u_{Ge}, v_{Ge}, and u_{Ni} (u_{Pt}), v_{Ni} (v_{Pt}). First we perform the optimization of the orthorhombic cell and internal parameters. Experimental and calculated NiGe and PtGe lattice constants, cohesive energy, and heat of formation are given in Table I. The internal in-plane parameters are in Table II, where the caption gives the atomic position in terms of the internal parameters. The calculated lattice constants are within 1–2% of reported experimental values.

Next we consider the electronic structure of bulk germanides. The energy bands of NiGe and PtGe along high-symmetry directions in the Brillouin zone are shown in Figs. 2(a) and 2(b), respectively. In Figs. 3(a) and 4(a), we show the total density of states of NiGe and PtGe, respectively. In Figs. 3(b) and 3(c), we show the partial density of states projected onto Ni and Ge atoms. In Figs. 4(b) and 4(c), we show the partial density of states projected onto Pt and Ge atoms, respectively. It is clear that the states at and just below the Fermi level are derived predominantly from the 3*d* (5*d*) orbitals of Ni (Pt) in the NiGe (PtGe) energy bands displayed in Figs. 2(a) and 2(b). It is interesting to note that the metallicity of PtGe appears almost accidental. The lower

TABLE I. Theoretical and experimental lattice constants, heat of formations, and cohesive energy for Ni, Pt, NiGe, PtGe, and Ge.

Material		a(Å)	b (A)	c (A)	E_{coh} (eV/atom)	ΔH_f (eV/atom)
Ni	Cal.	3.52			5.40	
	Exp.[a]	3.52			4.44	
Pt	Cal.	3.93			5.77	
	Exp.[a]	3.92			5.84	
NiGe	Cal.	5.84	5.36	3.50	4.90	−0.32
	Exp.[b]	5.79	5.37	3.43		
PtGe	Cal.	6.16	5.83	3.75	5.18	−0.48
	Exp.[c]	6.09	5.72	3.70		
Ge	Cal.	5.75			3.76	
	Exp.[a]	5.65			3.85	

[a]Reference 31.
[b]Reference 19.
[c]Reference 20.

TABLE II. Experimental and calculated free internal in-plane coordinates of NiGe and PtGe. The Ni (Pt) atoms are located at $[u_{Ni(Pt)}, v_{Ni(Pt)}, 1/4]$, $[(1/2-u_{Ni(Pt)}), (v_{Ni(Pt)}-1/2), 1/4]$, $[(1-u_{Ni(Pt)}), (1-v_{Ni(Pt)}), 3/4]$, and $[(1/2+u_{Ni(Pt)}), (3/2-v_{Ni(Pt)}), 3/4]$, while the Ge atoms are located at $[u_{Ge}, v_{Ge}, 1/4]$, $[(3/2-u_{Ge}), (1/2+v_{Ge}), 1/4]$, $[(u_{Ge}-1/2), (1/2-v_{Ge}), 3/4]$, and $[(1-u_{Ge}), (1-v_{Ge}), 3/4]$.

		$u_{Ni(Pt)}$	$v_{Ni(Pt)}$	u_{Ge}	v_{Ge}
NiGe	Exp.	-	-	-	-
	Cal.	0.1795	0.9933	0.5770	0.1769
PtGe	Exp.[a]	0.1908	0.9995	0.5900	0.1850
	Cal.	0.1922	0.9988	0.5884	0.1857

[a]Reference 20.

Ge *p*-derived band near the Fermi level is occupied only along the Γ-*Y* direction, and the upper *p*-derived band "touches" the Fermi level at *Z* and along *R*-Γ direction. Elsewhere along the high-symmetry directions a clear band gap is observed. Charge density contours for NiGe (001) and Ni (001) planes are shown in Figs. 5(a) and 5(b). As apparent from Fig. 5(a), there appear to be relatively strong three-center (Ni-Ge-Ni) covalent bonds between Ni and Ge atoms in the (001) plane. This is interesting since NiGe is metallic. It is well known that the bonding of transition metals is almost entirely due to the *d*-electrons. Thus, it is not unexpected that the Ni-*d* would hybridize with the Ge-*p* to form covalent bonds. This is very similar to the chemical bonding

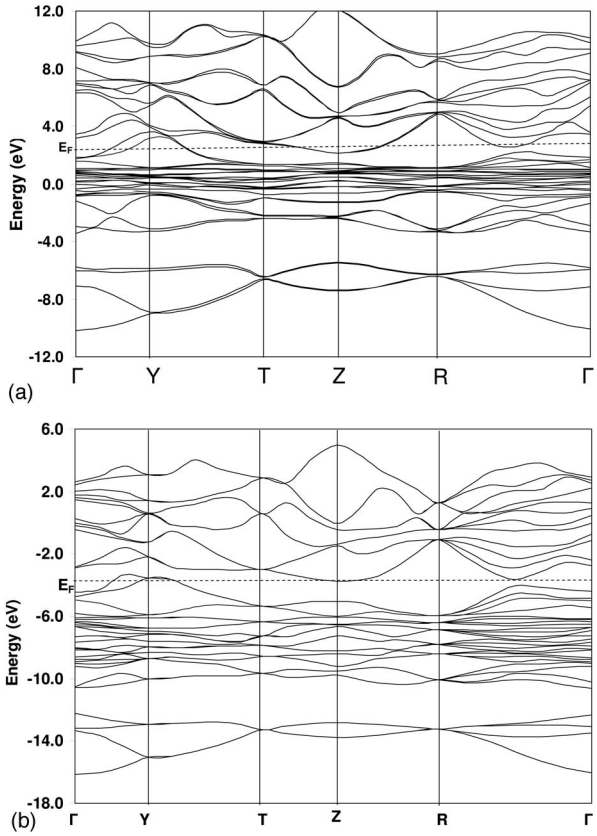

FIG. 2. Energy bands of (a) bulk NiGe and (b) bulk PtGe. The symmetry points are labeled according to Slater (Ref. 38).

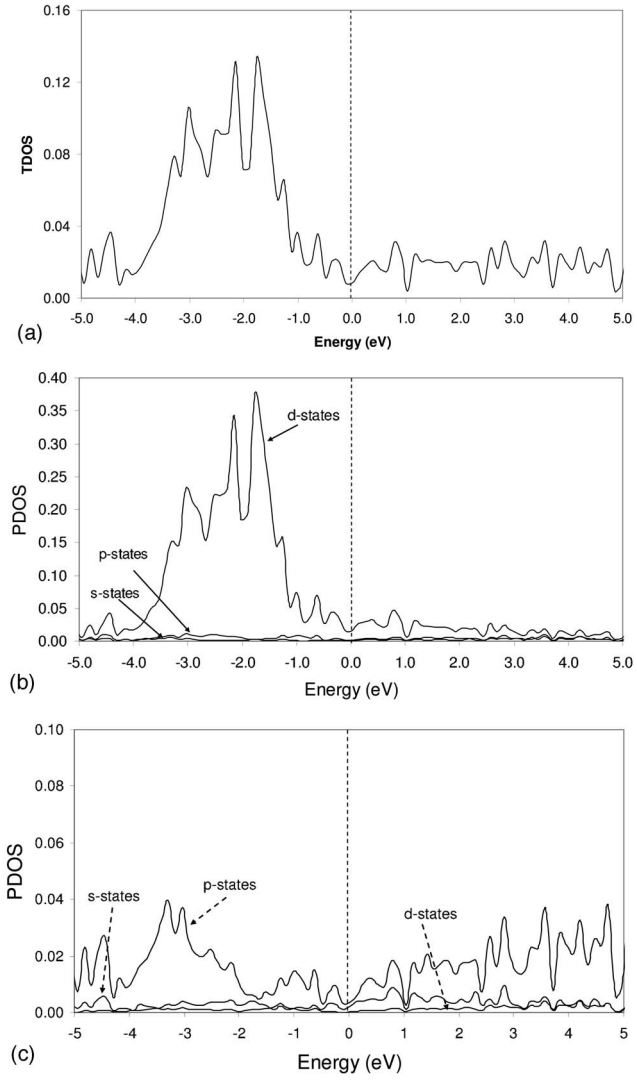

FIG. 3. (a) The total density of states of NiGe. (b) The partial density of states of NiGe projected onto Ni atoms. (c) The partial density of states of NiGe projected onto Ge atoms. Fermi energy is indicated by the dashed line, and amounts are given in electrons per Å^3 per eV for TDOS and electrons per Wigner-Seitz sphere per eV for PDOS.

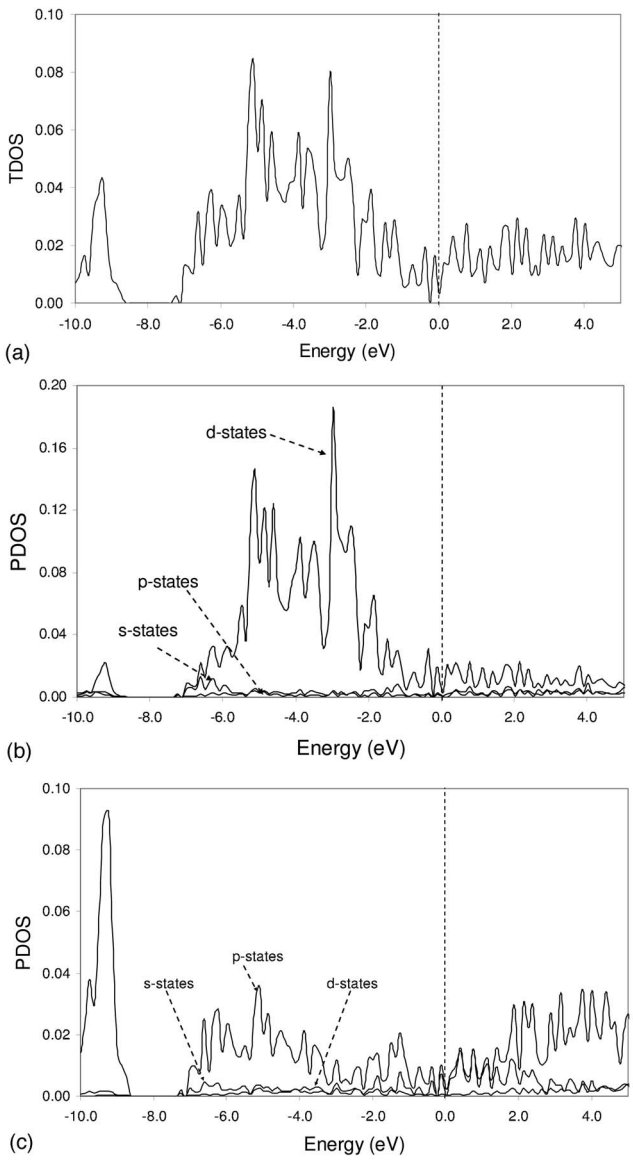

FIG. 4. (a) The total density of states of PtGe (b) The partial density of states of PtGe projected onto Pt atoms. (c) The partial density of states of PtGe projected onto Ge atoms. Fermi energy is indicated by the dashed line, and amounts are given in electrons per Å^3 per eV for TDOS and electrons per Wigner-Seitz sphere per eV for PDOS.

observed in PtSi.[23,24] The bonding in PtGe was found to be qualitatively similar to that in NiGe.

III. ELASTIC CONSTANTS

Thermal cycling during the Ge process is expected to be gentler than that of Si (during the activation of dopants a Si wafer is annealed at temperatures in excess of 1000 °C). Still a wafer will experience significant thermal stress, and knowing the elastic constants of germanide crystals is of practical importance. Nine elastic constants are needed to describe an orthorhombic crystal (compare with only three for a cubic crystal).[25] Our elastic constants were calculated by fitting the total energy as a function of strain to a parabola. The fit is based on six points separated by ~2 meV, and the applied strain is ~1% of the lattice constant. The procedure of calculating different elastic constants can be found in detail in Refs. 25 and 26. The experimental and calculated elastic constants of Si, Ge, Ni, Ge (fcc crystals) are given in Table III. The theoretical elastic constants and bulk moduli are within 5% of experiment. The calculated elastic constants of orthorhombic NiGe and PtGe are given in Table IV. Interestingly, despite the difference in crystal structure and nature of bonding, the values calculated for monogermanides are remarkably close to simple averages of the Ge and metal values. We have checked the convergence of the elastic constant C_{44} with respect to the number of k-points and plane wave energy cutoff (for NiGe). The value of C_{44} was raised by 0.7 and 2.1% as the k-point mesh is

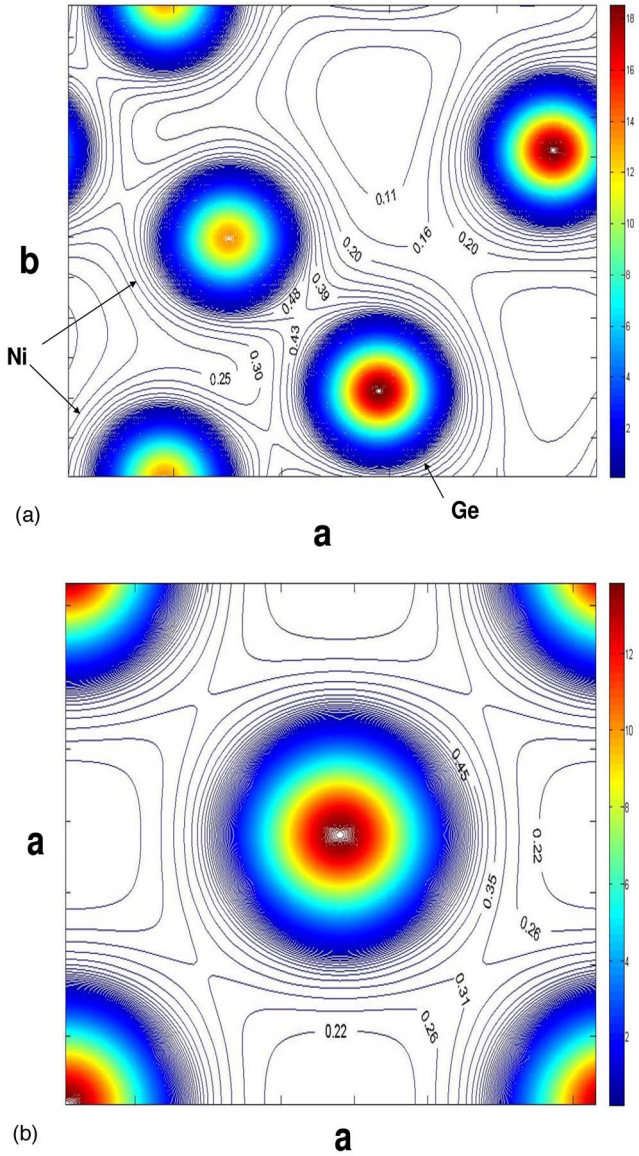

FIG. 5. (Color online) (a) Valance electron charge density (electrons/Å^3) contours in the (001) plane for (a) a NiGe unit cell and (b) a Ni unit cell.

increased from $6\times6\times8$ to $8\times8\times12$ and $10\times10\times16$. The C_{44} value was raised by 0.3 and 0.4% as the energy cutoff was increased from 380 eV to 530 eV and 640 eV, respectively. To further check the quality of our calculations we consider the issue of mechanical stability. The stability conditions for an fcc crystal restrict the elastic constants in the following way:[27]

$$(C_{11}-C_{12})>0, C_{11}>0, C_{44}>0, (C_{11}+2C_{12})>0 \text{ and } C_{12}<B<C_{11},$$

where B is the bulk modulus. For fcc crystals, such as Ni, Pt, Ge, and Si, the bulk modulus can be calculated as $B_0=1/3(C_{11}+2C_{12})$. To ensure the internal consistency we also calculate the bulk modulus and equilibrium volume by fitting the total energy as a function of volume to a parabola and a four-term Birch–Murnaghan equation of state:[28]

$$E(V)=\sum_{n=1}^{4} c_n V^{-2n/3}.$$

The bulk moduli calculated from the elastic constants, from a parabolic fit and Birch–Murnaghan fit, in addition to experimental values, are given in Tables III and IV. The calculated elastic constants of Ge, Si, Ni, and Pt lie well within the allowed range for mechanically stable fcc crystals. Likewise, the elastic constants of mechanically stable orthorhombic

TABLE III. Calculated and experimental elastic constants (in units of GPa) of Ge, Si, Ni, and Pt. Experimental values for Ge, Si, Ni, and Pt are extrapolated to 0 K. B_0 is the bulk modulus calculated from elastic constants and from Birch–Murnaghan fit. B_0 is related to elastic constants as $B_0=1/3(C_{11}+2C_{12})$. Superscript indicates the reference to the experimental values.

		Ni[a]	Pt[b]	Ge[c]	Si[d]
C_{11}	Cal.	268.4	334.6	124.2	159.8
	Exp.	261.2	358	131	165
C_{12}	Cal.	159.3	247.1	45.9	60.5
	Exp.	150.8	254	44	63
C_{44}	Cal.	131.2	72.2	71.3	75.2
	Exp.	131.7	77	68.8	79.1
B_0	Cal.$^{\text{Birch}}$	194.9	272.2	69.9	94.7
	Cal.$^{\text{parabolic}}$	195.3	275.8	70.8	94.2
	Cal.$^{\text{elastic}}$	195.7	276.3	72.0	93.6
	Exp.	187.6	288.4	76.3	97

[a]Reference 31.
[b]Reference 33.
[c]Reference 34.
[d]Reference 35.

TABLE IV. Calculated elastic constants and bulk modulus (in units of GPa) of NiGe and PtGe. $B^0_{elastic}$ is the bulk modulus calculated from the elastic constants and is given as $B^0_{elastic}=1/9(C_{11}+C_{22}+C_{33}+2C_{12}+2C_{13}+2C_{23})$. $B_0^{parabolic}$ and B_0^{Birch} are the bulk modulus obtained from a parabolic and Birch–Murnaghan fit.

	NiGe	PtGe
C_{11}	211.69	216.52
C_{22}	183.76	200.57
C_{33}	173.93	206.15
C_{12}	135.70	125.18
C_{13}	99.80	114.42
C_{23}	106.37	113.12
C_{44}	67.20	68.88
C_{55}	106.94	76.02
C_{66}	105.41	53.63
$B_0^{elastic}$	139.24	147.63
$B_0^{parabolic}$	140.58	153.41
B_0^{Birch}	140.94	154.62

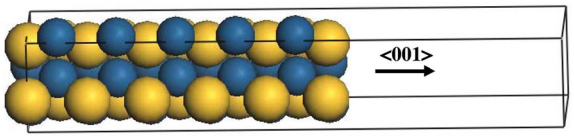

FIG. 6. (Color online) The simulation cell for the (001)-oriented NiGe (PtGe) surface slab. Larger light balls are Ge atoms, and smaller dark balls are Ni (Pt) atoms.

crystals are constrained by the following conditions:[27]

$$C_{11} > 0, C_{22} > 0, C_{33} > 0, C_{44} > 0, C_{55} > 0, C_{66} > 0,$$
$$(C_{11} + C_{22} - 2C_{12}) > 0,$$
$$(C_{11} + C_{33} - 2C_{13}) > 0,$$
$$(C_{22} + C_{33} - 2C_{23}) > 0,$$
$$(C_{11} + C_{22} + C_{33} + 2C_{12} + 2C_{13} + 2C_{23}) > 0, \text{ and}$$
$$1/3(C_{12} + C_{13} + C_{23}) < B < 1/3(C_{11} + C_{22} + C_{33}).$$

For orthorhombic NiGe and PtGe bulk modulus is first calculated as $B_0 = 1/9(C_{11}+C_{22}+C_{33}+2C_{12}+2C_{13}+2C_{23})$.[27] As evident from Table IV, the calculated elastic constants of NiGe and PtGe do obey conditions of mechanical stability. The rather poor agreement (relative to the fcc crystals) between the PtGe bulk modulus calculated from the elastic constants and the two bulk moduli calculated assuming hydrostatic pressure is undoubtedly due to the inner displacements of the atoms, and the need to equilibrate the stresses. That the agreement for NiGe is good may be fortuitous.

IV. SURFACE ENERGY AND RECONSTRUCTION OF NiGe AND PtGe

We calculate surface energies for (100), (010), (001), (011), (101), (111), (120), (121), (211), and (021) orientations of bulk NiGe and PtGe for different surface stoichiometries. To simulate the surfaces, we used supercells in slab geometry of thickness 14–20 Å (10–17 layers in addition to vacuum layers). For example, to simulate the NiGe (001) surface, we use eight layers of vacuum over eleven layers of NiGe (001) (shown in Fig. 6). The smallest (001)-oriented slab contains 44 atoms; the largest (121)-oriented slab contains 63 atoms. Symmetric slabs based on (1×1) surface cells for each termination are used (the lateral lattice constant is fixed to that derived from the calculated bulk value). For the Brillouin zone integration, we use a moderate $4\times4\times1$ Monkhorst–Pack[18] mesh, due to relatively large cell sizes. To check the convergence we perform calculations with $(6\times6\times1)$ and $(8\times8\times1)$ grids and find the energy changes are of the order of 10^{-4} eV/atom. Each supercell is relaxed until the forces on each atom reach 0.02 eV/Å or less.

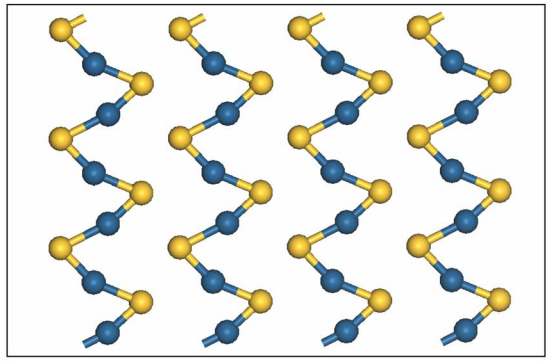

FIG. 7. (Color online) Top view of the unreconstructed NiGe (001) surface. Blue and yellow balls are Ni and Ge atoms, respectively.

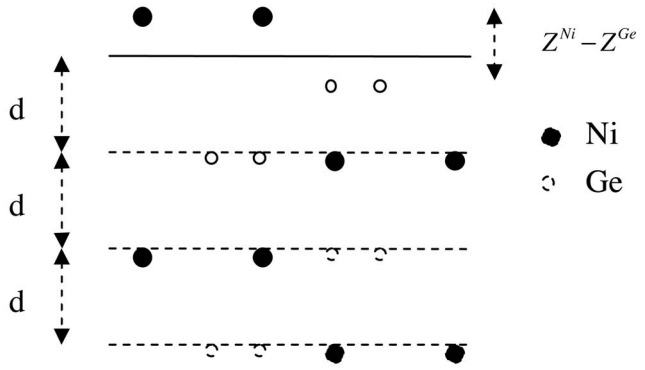

FIG. 8. NiGe (001) surface (side view).

Now we describe the nature of reconstruction of the NiGe (001)-1×1 surface. The NiGe (001) surface has a rectangular surface unit cell of dimensions 5.84 Å by 5.36 Å. There are two Ge and two Ni atoms in the surface. The unreconstructed surface can be described as zigzag NiGe chains running along the shorter cell edge (see Fig. 7). We define the rumpling parameter δr_i as in Ref. 24,

$$\delta r_i = (Z_i^{\mathrm{Ni}} - Z_i^{\mathrm{Ge}})/d_o,$$

where Z^{Ni} and Z^{Ge} are the z coordinates of the Ni and Ge atoms in the ith layer and d_0 is the bulk interlayer distance (Fig. 8). We also define the interplanar relaxation parameter δr_{ij} as

TABLE V. Surface rumpling and interplanar relaxation in percent for the NiGe (001) surface. The rumpling parameter δr_i is defined as $\delta r_i = (Z_i^{\mathrm{Ni}} - Z_i^{\mathrm{Ge}})/d_o$, where Z^{Ni} and Z^{Ge} are the z coordinates of the Ni and Ge atoms in the ith layer and d_0 is the bulk interlayer distance [Fig. 8(a)]. The interplanar relaxation parameter δr_{ij} is defined as $\delta r_{ij} = (Z_i - Z_j)/d_a$, where Z_i and Z_j are the z coordinates of the ith and jth layer and d_0 is the bulk interlayer distance. Z_i is calculated by averaging the z coordinates of the Ni and Ge atoms.

	δr_1	δr_2	δr_3	δr_4	δr_{12}	δr_{23}	δr_{34}	δr_{45}
Calc.	−9.8	2.0	−2.9	0.7	−4.8	0.6	0.0	0.0

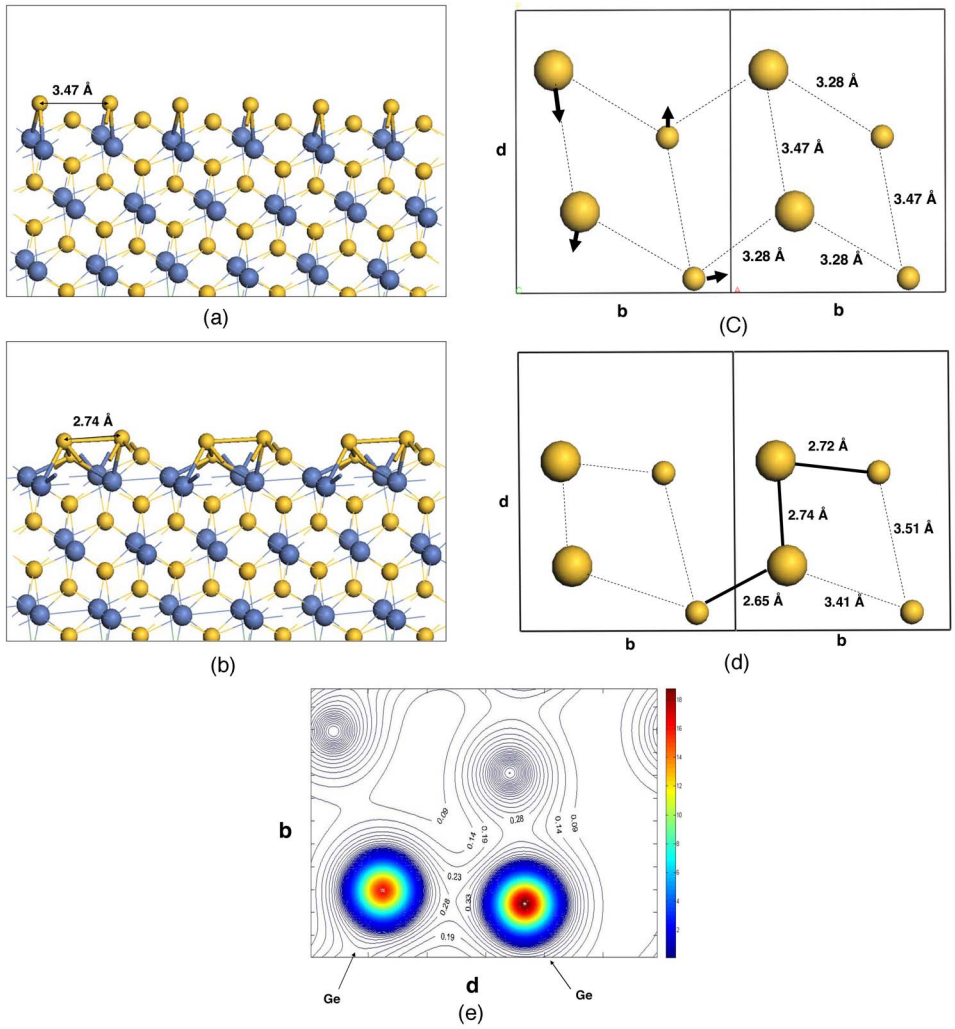

FIG. 9. (Color online) (a) Side view of the *unreconstructed* Ge-terminated NiGe (101) surface. Yellow and blue balls are Ge and Ni atoms, respectively. The top layer Ge atoms are twofold coordinated, and Ge-Ge distance is 3.47 Å. The structure is vaguely reminiscent of the Ge (001) unreconstructed surface (Ge-Ge separation is the second-nearest-neighbor distance of 3.99 Å). (b) Side view of the *reconstructed* Ge-terminated NiGe (101) surface. Yellow and blue balls are Ge and Ni atoms, respectively. The bonds formed in the surface layer are indicated with balls and sticks, while the rest of the slab is rendered with a wireframe. Top Ge atoms in the surface layer are fourfold coordinated with one bridging dimer bond in the surface plane one bond to the lower Ge and two back bonds to Ni atoms in the subsurface layer. The lower Ge atoms are fivefold coordinated; in addition to Ge-Ge bond with the top Ge, they form four back-bonds to subsurface Ni atoms. (c) Top view of the *unreconstructed* Ge-terminated NiGe (101) surface. Larger balls represent Ge atoms in the topmost layer, and smaller balls represent Ge atoms that lie in the plane 0.97 Å below. Two surface unit cells are shown, the lattice constants are $\boldsymbol{b}=5.36$ Å, $\boldsymbol{d}=6.81$ Å. There are no bonds between Ge atoms before the relaxation. The arrows indicate the movement of the atoms during relaxation. (d) Top view of the *reconstructed* Ge-terminated NiGe (101) surface. Larger balls represent Ge atoms in the topmost layer, and smaller balls represent those in the plane 0.87 Å below. Two surface unit cells are shown for clarity. The surface Ge-Ge bonds are indicated with thick black lines. Top Ge atoms form a 2.74 Å dimer bond with each other, and one similar and one shorter bond to lower plane surface Ge atoms, as well as two back-bonds to Ni atoms below. (e) Valance electron charge density (electrons/Å^3) contours at NiGe(101)-1×1 (Ge-terminated) reconstructed surface. The surface cell is (b,d), with d being equal to $\sqrt{a^2+c^2}$. The dimer Ge-Ge bond is clearly seen between two marked top Ge atoms, and a back-bond to the lower Ge atoms can also be seen.

$$\delta r_{ij} = (Z_i - Z_j)/d_a,$$

where Z_i and Z_j are the z coordinates of the ith and jth layer and d_a is the bulk interlayer distance. Z_i is calculated by averaging the z coordinate of the Ni (Pt) and Ge atoms. The interplanar distance in the bulk NiGe is 1.75 Å. The results for surface rumpling and interplanar relaxation are presented in Table V. In addition, we observe relatively small in-plane atomic displacements in the first two surface layers. The Ni and Ge atoms on the first surface layer are displaced by 0.01 Å and 0.11 Å, respectively. We did not consider the possibility of a more complex surface relaxation in a larger surface cell.

We have also studied the reconstruction of the germanium-terminated NiGe (101)-1×1 surface. As cut, the NiGe (101)-Ge terminated surface has two germanium at-

TABLE VI. Surface rumpling and interplanar relaxation in percent for the NiGe (101) surface. Subscripts 1, 2, 5, and 6 correspond to Ge layers, while subscripts 3, 4, and 7 correspond to Ni layers.

	δr_1	δr_2	δr_3	δr_4	δr_5	δr_6	δr_7	δr_{12}	δr_{23}	δr_{34}	δr_{45}	δr_{56}	δr_{67}
Calc.	14	1.3	11.7	10.2	4.8	3.7	0.3	−4.1	7.7	−46.4	14.2	−2.6	4.4

oms at the top layer and two Ge atoms at the layer 0.97 Å below it [see Fig. 9(a)]. Due to the strong covalent character of Ni-Ge bonds it is not unreasonable to describe the top-layer Ge atoms as having two "bonds" to Ni atoms in the subsurface layer and the lower-layer ones as having four (the bond length is ~2.46 Å). The geometry in the top layer is vaguely reminiscent of an as-cut Ge (001) (1×1) surface, which, as is well known, is unstable with respect to a (2×1) reconstruction caused by dimerization. As apparent from Figs. 9(b)–9(e), topmost germanium atoms at the NiGe (101) surface also tend to dimerize. This is rather interesting since dimerization (or any significant surface relaxation) is not very common for metallic surfaces with the notable exception of Au. Note that the cell remains (1×1). The separation between top Ge atoms is decreased from 3.28 Å to 2.71 Å, suggesting formation of a dimer upon reconstruction [see Fig. 9(b)]. Overall, however, the reconstruction is more complicated and can be described as follows. In Fig. 9(c) we show the rhombus formed by four unreconstructed surface Ge atoms; note that there are no Ge-Ge bonds. Upon reconstruction, two top Ge atoms bond with each other, and also with two lower Ge atoms [see Fig. 9(d)]. As can be seen from Fig. 9(e) the surface Ge-Ge bonds are covalent. In addition, Ge atoms form back bonds to Ni in the subsurface layer ranging from 2.45 to 2.79 Å in length. Furthermore, the energy gained in this unusual reconstruction process is 1.70 eV or 0.85 eV per surface, which is significant, and about 50% of the cohesive energy of bulk Ge per covalent bond. The results for surface rumpling and interplanar relaxation are presented in Table VI. Importantly, this surface is also the lowest energy surface of orthorhombic NiGe.

The surface energy of a NiGe or PtGe surface is estimated using the Gibbs free energy approach.[29,30] We have previously used this method to evaluate surface energy of PtSi and refer the reader to that paper for more details.[24] For example, the surface free energy of NiGe is given by

$$E=\tfrac{1}{2}(E_{Slab}-N_{\mathrm{Ge}}E_{\mathrm{Ge}}-N_{\mathrm{Ni}}E_{\mathrm{Ni}}+N_{\mathrm{Ge}}E_{form}+\mu_{\mathrm{Ni}}(N_{\mathrm{Ge}}-N_{\mathrm{Ni}}),$$

where E_{Slab} is the total energy of the supercell, and E_{Ge} and E_{Ni} are the energies per atom of bulk Ge and Ni, respectively. N_{Ge} (N_{Ni}) and μ_{Ge} (μ_{Ni}) are the number of Ge (Ni) atoms and Ge (Ni) chemical potential, respectively. Chemical potentials of Ni and Ge are taken with respect to the bulk phases and the surface is assumed to be in equilibrium with bulk NiGe [thus, μ_{Ge} and μ_{Ni} are related by the equilibrium condition: $\mu_{\mathrm{Ge}}+\mu_{\mathrm{Ni}}=-E_{form}(\mathrm{NiGe})$]. The energy is given per unit surface cell, and a factor of 1/2 is inserted to account for two surfaces in the supercell.

The surface energies of different NiGe and PtGe surfaces are tabulated in Table VII and VIII, respectively. In Figs. 10(a) and 10(b), we show surface energies of different NiGe and PtGe terminations as a function of the Ni or Pt chemical potential. The zero value of the chemical potential corresponds to metal (Ni or Pt) rich conditions; beyond that point metallic Ni (Pt) will start forming on the surface. The range

TABLE VII. Surface energies and work functions for different NiGe surface orientations. Superscripts g and n refer to the Ge- and Ni-terminated surfaces.

Surface	Surface Energy (erg/cm^2)	Work Function (eV)
NiGe(100)^n	1879.03−426.22 μ_{Ni}	4.31
NiGe(100)^g	1505.90+426.22 μ_{Ni}	4.53
NiGe(010)^n	1828.33−000.00 μ_{Ni}	4.37
NiGe(110)^n	1460.20+000.00 μ_{Ni}	4.51
NiGe(110)^g	1310.63+000.00 μ_{Ni}	4.76
NiGe(001)	1401.08−000.00 μ_{Ni}	4.57
NiGe(120)^n	1598.74−177.78 μ_{Ni}	4.64
NiGe(120)^g	1630.74+177.78 μ_{Ni}	4.57
NiGe(211)^n	1419.26−150.91 μ_{Ni}	4.55
NiGe(211)^g	1300.27+150.91 μ_{Ni}	4.55
NiGe(021)^n	1424.50−000.00 μ_{Ni}	4.65
NiGe(101)^n	1975.93−875.77 μ_{Ni}	4.39
NiGe(101)^g	1504.37+875.77 μ_{Ni}	4.58
Ni(111)		5.09, 5.35[a]

[a]Experimental value of Ref. 36.

TABLE VIII. Surface energies and work functions for different PtGe surface orientations. Superscripts g and p refer to the Ge- and Pt-terminated surfaces.

Surface	Surface energy (erg/cm^2)	Work Function (eV)
PtGe(100)^p	1338.87−365.31 μ_{Pt}	4.95
PtGe(110)^p	1112.11+000.00 μ_{Pt}	4.88
PtGe(001)	1110.09−000.00 μ_{Pt}	4.83
PtGe(010)^p	1121.33−345.95 μ_{Pt}	5.01
PtGe(111)^p	1172.86−166.64 μ_{Pt}	4.88
PtGe(120)^p	1143.16−156.33 μ_{Pt}	4.93
PtGe(021)^p	1102.70−000.00 μ_{Pt}	4.97
PtGe(101)^p	1268.19−380.30 μ_{Pt}	4.91
PtGe(101)^g	1398.32+380.30 μ_{Pt}	4.58
PtGe(110)^g	1015.69+000.00 μ_{Pt}	4.87
PtGe(100)^g	1387.50+365.30 μ_{Pt}	4.59
Pt(111)		5.70, 5.70[b]

[b]Experimental value of Ref. 37.

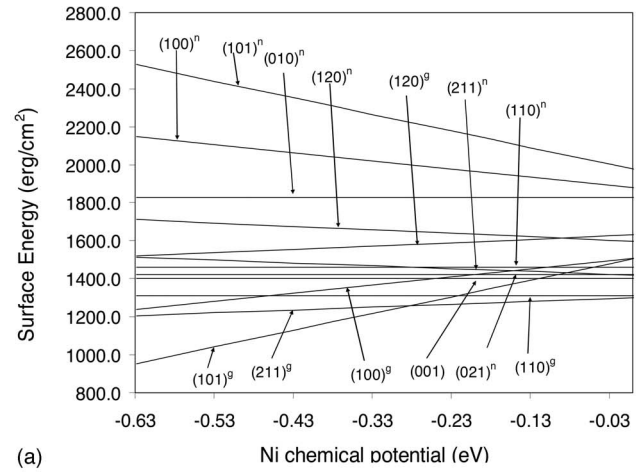

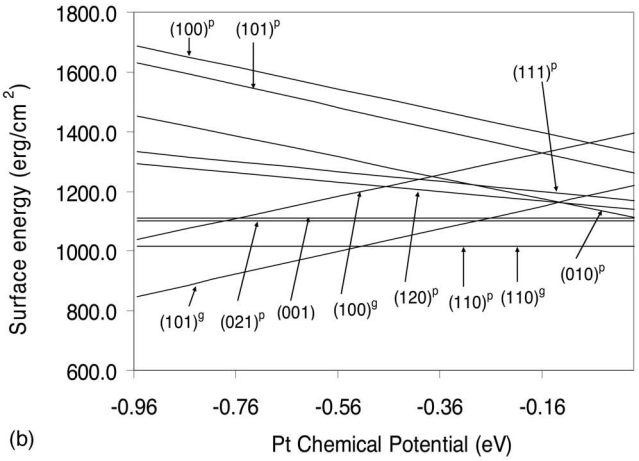

FIG. 10. (a) Surface energies of NiGe surfaces as a function of Ni chemical potential. Surfaces with superscript *n* refer to Ni-terminated surfaces while surfaces with superscript *g* refer to Ge-terminated surfaces. Surfaces without any superscripts are stoichiometric. (b) Surface energies of PtGe surfaces as a function of Pt chemical potential. Surfaces with superscript "p" refer to Pt-terminated surfaces, while surfaces with superscript *g* refer to Ge-terminated surfaces. Surfaces without any superscripts are stoichiometric.

is bound by the NiGe formation energy; Ge would start forming on the surface should this value be exceeded. Not surprisingly, as can be seen from Fig. 10(a), the germanium-terminated (101) surface remains most stable under most growth conditions while the germanium-terminated (211) surface becoming the most stable under extremely Ni-rich conditions. We also notice that under Ge-rich conditions, while (101) is still the lowest energy surface, several terminations such as germanium-terminated (110), (211), and (100), nickel-terminated (211), and stoichiometric (001) and (021) are very close in energy, and are only 200 erg/cm^2 higher than Ge-terminated (101). Overall, the Ni-rich termination is less stable than the stoichiometric termination, which in turn is less stable than the Ge-rich one throughout the thermodynamically accessible range.

In the case of PtGe, the germanium-terminated (101) orientation appears to be most stable under most of the growth conditions, while Ge- and Pt-terminated (110) surfaces become more stable when growth conditions are Pt-rich [Fig. 10(b)]. Under Ge-rich conditions (when germanide formation presumably takes place), the next stable surface is Ge- and Pt-terminated (110). Again, the general trend is that the Ge-terminated surface is most stable, followed by the stoichiometrically terminated and finally, metal-terminated surface.

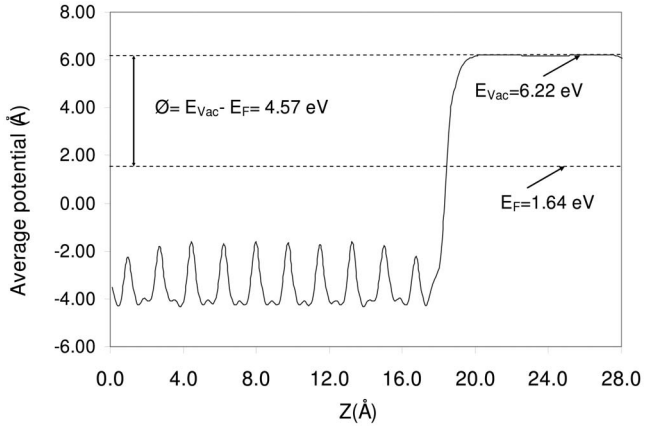

FIG. 11. The planar averaged Coulombic potential and work function of the NiGe (001) surface. *Z* is the direction normal to the (001) surface.

V. WORK FUNCTION AT DIFFERENT NiGe AND PtGe SURFACES

The work function φ_m at a metal surface is defined as energy needed to remove an electron from the bulk to the vacuum just outside the metal.[31] It is generally known that the work function changes with the orientation of the metal surface by amounts ranging from 1/10 to 1 eV. This anisotropy is generally attributed to the redistribution of the charge density at the surface, resulting in a different dipole barrier. As was first suggested by Smoluchowski,[32] there are two competing effects on the dipole layer which tend to raise and lower the magnitude of the work function. The first effect is the charge spilling out at the surface, resulting in the formation of a negative dipole layer (dipole pointing inward to the surface), which increases the work function. The second effect is the tendency to smooth out the surface, resulting in the formation of a positive dipole layer, which tends to lower the work function. Since these two effects are comparable in magnitude, the net surface dipole magnitude can only be determined numerically. Within the DFT-GGA formalism, the work function can be readily calculated in slab geometry as $\varphi_m = E_{Vac} - E_{Fermi}$. Here E_{Vac} and E_{Fermi} are the vacuum energy and the Fermi level. The vacuum energy E_{Vac} is estimated by the value of the total electrostatic potential in the vacuum region separating periodic images of the slab. The use of the electrostatic component only is justified since the exchange potential can be ignored in the middle of the vacuum region where its true value is zero.

We calculate work functions for different surface orientations and terminations of NiGe and PtGe surfaces (listed in Tables V and VI) using the value of the planar average of the

total electrostatic potential at the middle of the vacuum region as E_{Vac}, as shown in Fig. 11. For example, the calculated vacuum energy and Fermi energy for the NiGe (001) surface are 6.22 eV and 1.64 eV, giving the work function of 4.57 eV. The highest φ_m value of 4.76 eV for NiGe is found for the Ge-terminated (110) surface and the lowest of 4.31 eV for the (100) Ni-terminated surface (it has the highest surface energy of all terminations considered); they differ by almost 0.45 eV. Surprisingly, the stoichiometry of the termination (Ge- vs Ni-rich) does not show a systematic effect on the work function. The lowest energy NiGe surface Ge-terminated (101) has a work function of 4.58 eV. We find that under the process relevant Ge-rich conditions, three lowest energy terminations, Ge-rich (101), (211), and (100), have practically identical work function of about 4.55 eV.

For PtGe the highest φ_m value of 5.01 eV is found for the (010) metal-rich surface and the lowest of 4.58 eV for the Ge-terminated (101) surface, which differ by 0.43 eV. The Ge-terminated surfaces all have lower work functions than the Pt-terminated ones. Also, the values for the metal-terminated PtGe surfaces are distributed over a narrow 0.07 eV range around the average value of 4.94 eV. However, since the germanide growth takes place under Ge-rich conditions, we expect a lower value of 4.6 eV will be reported. Unfortunately, we know of no experimental data for NiGe and PtGe work functions. To gauge the reliability of our calculated results we calculate the work function of the Ni (111) and Pt (111) surfaces and obtained φ_m=5.09 eV and φ_m=5.70 eV. The experimental values reported in the literature for these surfaces are 5.35 eV[36] and 5.70 eV,[37] respectively.

VI. CONCLUSION

With the aid of density functional theory, we have studied the electronic structure of NiGe and PtGe, calculating work functions and surface energies for various surface terminations. Ge-terminated surfaces are found to have lowest surface energies, closely followed by the stoichiometrically terminated surfaces, while metal-rich terminations have much higher energy. We find that the work functions of NiGe and PtGe vary by as much as 0.45 eV and 0.43 eV, respectively, depending on the orientation. However, under Ge-rich conditions the lowest energy surface terminations would result in the same work function of about 4.6 eV for both germanides, regardless of orientation. For the Ge-rich (101) termination we identify a surface reconstruction unusual for metals, which results in the formation of Ge dimers akin to those observed on the (100) surface of Ge. The dimer bonding appears to be partially covalent. This reconstruction produces the lowest energy surface.

ACKNOWLEDGMENTS

This work was supported by the Semiconductor Research Corporation under Contract 2006-JV-1439, the Welch Foundation under Grant No. F-0934, and Texas Advanced Computing Center. M.N. thanks SEMATECH, Austin, for summer support through the Summer Internship program.

*Email address: demkov@physics.utexas.edu

[1] C. Detavernier, A. S. Özcan, J. Jordan-Sweet, E. A. Stach, J. Tersoff, F. M. Ross, and C. Lavoie, Nature (London) **426**, 641 (2003).
[2] M. L. Lee, E. A. Fitzgerald, M. T. Bulsara, M. T. Currie, and A. Lochtefeld, J. Appl. Phys. **97**, 011101 (2005).
[3] H. Shang, H. Okorn-Schimdt, J. Ott, P. Kozlowski, S. Steen, E. C. Jones, H.-S. P. Wong, and W. Hanesch, IEEE Electron Device Lett. **24**, 242 (2003).
[4] H. Shang, K.-L Lee, P. Kozlowski, C. D'Emic, I. Babich, E. Sikorski, I. Meikei, H.-S. P. Wong, K. Guarini, and W. Haensch, IEEE Electron Device Lett. **25**, 135 (2004).
[5] A. Ritenour, A. Khakifirooz, D. A. Antoniadis, R. Z. Lei, W. Tsai, A. Dimoulas, G. Mavrou, and Y. Panayiotatos, Appl. Phys. Lett. **88**, 132107 (2006).
[6] N. Wu, Q. Zhang, C. Zhu, D. S. H Chan, A. Du, N. Balasubramanian, M. F. Li, A. Chin, J. K. O. Sin, and D.-L. Kwong, IEEE Electron Device Lett. **25**, 631 (2004).
[7] J. Bardeen and W. H. Brattain, Phys. Rev. **74**, 230 (1948).
[8] G. D. Wilk, R. M. Wallace, and J. M. Anthony, J. Appl. Phys. **89**, 5243 (2001).
[9] Huang *et al.*, Tech. Dig. - Int. Electron Devices Meet. **2003**, 13.4.1.
[10] S. Zhu, L. Rui, S. J. Lee, M. F. Li, A. Du, J. Singh, C. Zhu, A. Chin, and D. L. Kwong, IEEE Electron Device Lett. **26**, 81 (2005).
[11] D. Z. Chi, R. T. P. Lee, S. J. Chua, S. J. Lee, S. Ashok, and D.-L. Kwong, J. Appl. Phys. **97**, 113706 (2005).
[12] D. M. Bylander and Leonard Kleinman, Phys. Rev. B **41**, 7868 (1990).
[13] P. Hohenberg and W. Kohn, Phys. Rev. **136**, B864 (1964).
[14] W. Kohn and L. J. Sham, Phys. Rev. **140**, A1133 (1965).
[15] P. E. Blöchl, Phys. Rev. B **50**, 17953 (1994).
[16] G. Kresse and J. Furthmuller, Phys. Rev. B **54**, 11169 (1996).
[17] J. P. Perdew, K. Burke, and M. Ernzerhof, Phys. Rev. Lett. **77**, 3865 (1996).
[18] H. J. Monkhorst and J. D. Pack, Phys. Rev. B **13**, 5188 (1976).
[19] J. Y. Spann, R. A. Anderson, T. J. Thornton, G. Harris, and C. Tracy, IEEE Electron Device Lett. **26**, 151 (2005).
[20] E. J. Graber, R. J. Baughman, and B. Morosin, Acta Crystallogr., Sect. B: Struct. Crystallogr. Cryst. Chem. **B29**, 1991 (1973).
[21] B. Balakrisnan, C. C. Tan, S. L. Liew, P. C. Lim, G. K. L. Goh, Y. L. Foo, and D. Z. Chi, Appl. Phys. Lett. **87**, 241922 (2005).
[22] R. Nath, C. W. Soo, C. B. Boothroyd, M. Yeadon, D. Z. Chi, H. P. Sun, Y. B. Chen, X. Q. Pan, and Y. L. Foo, Appl. Phys. Lett. **86**, 201908 (2005).
[23] N. Franco, J. E. Klepeis, C. Bostedt, T. Van Buuren, C. Heske, O. Pankratov, T. A. Callcott, D. L. Ederer, and L. J. Terminello, Phys. Rev. B **68**, 045116 (2003).
[24] M. K. Niranjan, S. Zollner, L. Kleinman, and A. A. Demkov,

Phys. Rev. B **73**, 195332 (2006).
[25] P. Ravindran, L. Fast, P. A. Korzhavyi, B. Johansson, J. Wills, and O. Eriksson, J. Appl. Phys. **84**, 4891 (1998).
[26] O. Beckstein, J. E. Klepeis, G. L. W. Hart, and O. Pankratov, Phys. Rev. B **63**, 134112 (2001).
[27] F. J. Nye, *Physical Properties of Crystals* (Oxford University Press, Oxford, 1985).
[28] E. Birch, J. Geophys. Res. **83**, 1257 (1978).
[29] J. Padilla and D. Vanderbilt, Surf. Sci. **418**, 64 (1998).
[30] G. X. Qian, R. M. Martin, and D. J. Chadi, Phys. Rev. B **38**, 7649 (1988).
[31] C. Kittel, *Introduction to Solid State Physics*, 6th ed. (Wiley, New York, 1986).
[32] R. Smoluchowski, Phys. Rev. **60**, 661 (1941).
[33] R. E. MacFarlane *et al.*, Phys. Lett. **18**, 91 (1965).
[34] M. E. Fine, J. Appl. Phys. **26**, 862 (1995).
[35] *Low Frequency Properties of Dielectric Crystals*, edited by D. F. Nelson, Landolt-Bornstein, New Series, Group III, Vol. 29a (Springer, Berlin, 1992).
[36] B. G. Baker, B. B. Johnson, and G. L. C. Maire, Surf. Sci. **24**, 572 (1971).
[37] M. Kiskinova, G. Pirug, and H. P. Bonzel, Surf. Sci. **133**, 321 (1983).
[38] J. C. Slater, *Symmetry and Energy Bands in Crystals*, Dover ed. (Dover, New York, 1972).